Acknowledgment. We thank the National Science Foundation for support of this research and for a grant that allowed purchase of the Convex C-2 computer, on which some of these calculations were performed. We also thank the San Diego Supercomputer Center for a generous allocation of computer time.

Supplementary Material Available: Tables of the RHF optimized geometries and energies of the closed shell molecules and the UHF geometries and energies of the radicals that appear in Table I (3 pages). Ordering information is given on any current masthead page.

An ab Initio MO Study on Ethylene and Propylene Insertion into the Ti-CH_3 Bond in $CH_3TiCl_2^+$ as a Model of Homogeneous Olefin Polymerization

Hiroshi Kawamura-Kuribayashi,[†,‡] Nobuaki Koga,[†] and Keiji Morokuma*[,†]

Contribution from the Institute for Molecular Science, Myodaiji, Okazaki 444, Japan, and Chiba Research Laboratory, Sumitomo Chemical Co., Ltd., 2-1 Kitasode Sodegaura Chiba 299-02, Japan. *Received April 11, 1991*

Abstract: As a model of olefin polymerization by a homogeneous Ziegler-Natta catalyst, the mechanism of the insertion reaction of ethylene and propylene into $CH_3TiCl_2^+$ has been studied by the ab initio MO method. The structures of the reactant, the intermediate, the transition state, and the product have been optimized with the RHF/3-21G (Ti:MIDI4) method. The transition state is four-centered and is slightly nonplanar to avoid C-H bond eclipsing. In the product strong C^{β}-C^{γ} and C-H agostic interactions take place to donate electrons to Ti vacant d orbitals. The energetics calculated at the unrestricted second-order Møller-Plesset perturbation level with double spin projection (DPUMP2) shows that the reaction proceeds via an ethylene complex with a binding energy of 45 kcal/mol and through the transition state with an activation energy from the ethylene complex of about 4 kcal/mol. In propylene polymerization, the barrier is higher than in ethylene insertion, and the primary insertion is easier than the secondary insertion, both consistent with experiments. The energy decomposition analysis indicates that these chemo- and regioselectivities are controlled by electrostatic and exchange (steric) interactions. The nonplanarity of the transition state makes one of two stereospecific primary insertion pathways substantially more favorable than the other; this tendency of a nonplanar transition state may have significance in determining stereospecificity in olefin polymerizations.

I. Introduction

The discovery of Ziegler-Natta polymerization in 1953 is one of the most important achievements in the field of synthetic polymer chemistry during the past half-century. For this olefin polymerization, a heterogeneous as well as homogeneous catalyst has been adopted. Heterogeneous catalysts are usually transition metal halides with cocatalysts such as aluminum alkyl compounds and electron donors; an example of such a combination studied experimentally very extensively is $TiCl_3$ + $(C_2H_5)_2AlCl$ + aromatic ester.[1-5] Homogeneous catalysts, on the other hand, are metallocenes,[6-9] transition metal dihalide dialkoxides[10] (e.g., $(RO)_2TiCl_2$), and metal tetraalkyls,[11,12] which are soluble in hydrocarbon solvent.

The mechanism proposed by Cossee[13] has been accepted widely as the most plausible, though it is very generic and qualitative. This mechanism is illustrated for Ti in Scheme I. The first step is olefin coordination to a vacant site of Ti. In the second step olefin inserts into the Ti-C bond through a four-membered cyclic transition state. This newly grown alkyl Ti species reinitiates olefin coordination and thus the propagation step.

Based on this mechanism, many MO theoretical studies have been carried out for this catalytic system.[14-24] In the earliest ab initio MO study, Novaro, Clementi, and co-workers[20] calculated the energy profile and analyzed briefly the electronic structure for each step of this mechanism with assumed geometries. Fujimoto and co-workers used a model cationic reaction (eq 1) with

$$\underset{\mathbf{1}}{CH_3TiX_2^+} + CH_2{=}CHR \rightarrow \underset{\mathbf{2}}{CH_3TiX_2(CH_2{=}CHR)^+} \rightarrow [\underset{\mathbf{3}}{\text{transition state}}] \rightarrow \underset{\mathbf{4}}{C_3H_6RTiX_2^+} \quad (1)$$

Scheme I

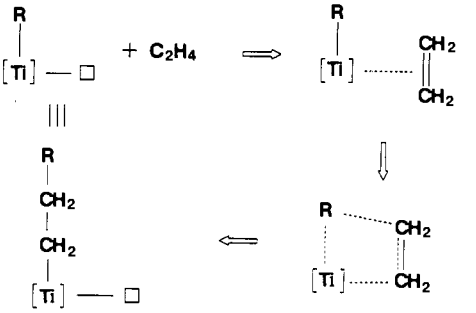

X = Cl for ethylene insertion (R = H) and optimized the transition structure with the ab initio restricted Hartree-Fock (RHF) method

[†] Institute for Molecular Science.
[‡] Sumitomo Chemical Co., Ltd.

(1) Keii, T. *Kinetics of Ziegler-Natta Polymerization*; Kodansha: Tokyo, 1972.
(2) Boor, J., Jr. *Ziegler-Natta Catalysts and Polymerization*; Academic Press: New York, 1979.
(3) Kissin, Y. V. *Isospecific Polymerization of Olefins*; Springer-Verlag: New York, 1985.
(4) Allen, G. B. *Comprehensive Polymer Science*; Pergamon Press: Oxford, 1989.
(5) Choi, K.; Ray, W. H. *Rev. Macromol. Chem.* **1985**, *C25*, 1, 57.
(6) Ewen, J. A. *J. Am. Chem. Soc.* **1984**, *106*, 6355.
(7) Kaminsky, W.; Kulper, K.; Brintzinger, H. H.; Wild, F. R. W. P. *Angew. Chem., Int. Ed. Engl.* **1985**, *24*, 507.
(8) Ewen, J. A.; Jones, R. L.; Razavi, A.; Ferrara, J. D. *J. Am. Chem. Soc.* **1988**, *110*, 6255.
(9) Miya, S.; Mise, T.; Yamazaki, H. *Chem. Lett.* **1989**, 1853.
(10) Miyatake, T.; Mizunuma, K.; Seki, Y.; Kakugo, M. *Makromol. Chem., Rapid Commun.* **1989**, *10*, 349.
(11) Ballard, D. G. H.; Van Lienden, P. W. *Makromol. Chem.* **1972**, *154*, 177.
(12) Ballard, D. G. H.; Dawkins, J. V.; Key, J. M.; Van Lieden, P. W. *Makromol. Chem.* **1973**, *165*, 173.

0002-7863/92/1514-2359$03.00/0 © 1992 American Chemical Society

under the C_s symmetry constraint.[21] Additionally Fujimoto et al. analyzed the main orbital interaction between the Ti complex and ethylene with the paired interacting orbital (PIO) method.[25] Another PIO analysis by Shiga and co-workers[22] has examined the effect of the number of valence electrons.

Marynick and collaborators recently studied with the PRDDO approximation the same model insertion reaction with chlorides or cyclopentadienyls as ligands (R = H, X = Cl, Cp).[23,24] When the ligands are chlorides, their optimized geometries are similar to Fujimoto's. They also carried out an ab initio restricted second-order Møller–Plesset (RMP2) calculation for X = Cp and claimed their activation barrier was in excellent agreement with the estimated experimental barrier. As will be discussed later, however, we find that the RHF wave function of $CH_3TiCl_2^+$ is unstable due to the triplet instability,[26] and we feel that RMP2 is not suitable for a reliable energetics for X = Cl. The structure determination of the transition states has been carried out only in a few cases mentioned above. Even in such studies a symmetry restriction was imposed, resulting in unfavorable eclipsed C–H bonds. Therefore, it is quite possible that olefin insertion actually passes through a transition state having a lower symmetry.

As has just been discussed, there has not been a full theoretical understanding of the olefin insertion reaction. Therefore, the first purpose of the present study is more complete determination of the potential energy surface for the olefin insertion of eq 1 (R = H and X = Cl) using better basis sets, including the effect of the correlation and without symmetry restriction. In fact, as will be shown below, we have found that the transition state is noncoplanar, contrary to what has been assumed.

The second purpose of the present study is an analysis of regio- and stereochemistry in propylene polymerization. No such MO study has been carried out. The regioselectivity is known to obey the Markovnikov rule; the primary insertion is preferred over the secondary insertion.[1-5] The stereochemistry of methyl groups in polypropylene, such as isotacticity, is a very important property of polymers and is also determined in the insertion process. Recently some homogeneous catalysts were paid much attention in this regard, because they were found to yield polymers with good stereospecificity in α-olefin polymerizations. For example, highly isotactic polypropylene has been obtained with the silylene-bridged metallocene catalyst,[9] and Ewen's catalyst gives syndiotactic polypropylene.[8] A chain-end control mechanism has been proposed by Zambelli for isotactic propagation based on experimental observation.[27] Corradini and co-workers calculated the Lennard-Jones-type nonbonded interaction energy between a Ti complex and olefin in an assumed model and supported Zambelli's suggestions qualitatively.[28] A realistic model of transition state and a reliable estimation of electronic energy would be required for theoretical discussion of the small energy difference in regio- and stereoselectivity. In the present study we used the transition state for ethylene insertion as a model, and estimated and analyzed the energetics for regio- and stereoselective insertion of propylene.

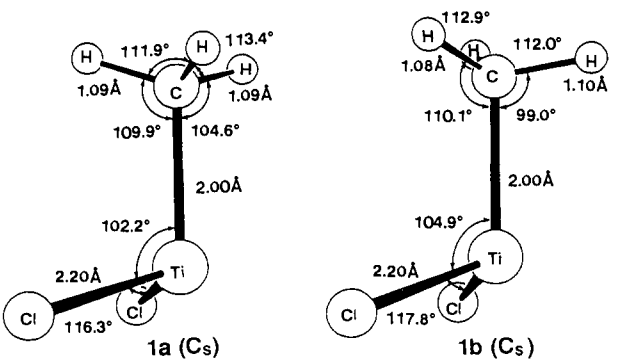

Figure 1. Optimized geometries of the reactant, $CH_3TiCl_2^+$, at the RHF/I level, under the C_s symmetry constraint.

We chose this reaction as a model of the propagation step in homogeneous polymerizations, in which Cp_2MR^+ has been considered to be a reactive intermediate for group 4 transition metal catalysts such as titanocene and zirconocene.[29] Eisch and his co-workers isolated $[Cp_2TiC(SiMe_3)=C(Ph)Me]^+AlCl_4^-$, in the reaction of $Me_3SiC\equiv CPh$ with Cp_2TiCl_2 and $MeAlCl_2$ and carried out the X-ray structure determination.[30] They proposed that in this reaction $Me_3SiC\equiv CPh$ inserts into the TiC bond of the reactive intermediate, $Cp_2TiCH_3^+$, and therefore they concluded that this is a model of the Ziegler polymerization. Very recently, Marks and co-workers reported the highly active "cation-like" zirconocene catalyst, $[Cp_2ZrCH_3]^+CH_3B(C_6F_5)_3^-$,[29] in which $[Cp_2ZrCH_3]^+$ weakly coordinates to $CH_3B(C_6F_5)_3^-$.

On the other hand, our model intermediate, $CH_3TiCl_2^+$, has Cl in place of Cp, and thus one may worry that $CH_3TiCl_2^+$ might be too electron deficient. In a previous theoretical study of the rearrangement between $X_2Ti(CH_2)(CH_2=CH_2)$ and $X_2Ti(CH_2CH_2CH_2)$, Upton and Rappé used Cl as X to replace Cp and as a result they found that this replacement gives a reasonable structure model.[31] As shown later, in $CH_3TiCl_2^+$, Ti, C, and two Cl are not coplanar. Marynick et al. have found a similar structure for the same molecule but a different structure for $Cp_2TiCH_3^+$, in which the methyl carbon, Ti, and the centroids of Cp are almost coplanar.[23,24] Based on these results, Marynick et al. concluded that $CH_3TiCl_2^+$ is not appropriate as a model intermediate. In our theoretical study[32] of $X_2Ti(C(SiH_2CH_3)=CH_2)^+$, the noncopolanar structure obtained for X = Cl is in much better agreement with the X-ray structure of $[Cp_2TiC(SiMe_3)=C(Ph)Me]^+AlCl_4^-$ shown above than the almost coplanar structure obtained for X = Cp. Thus, we believe that the model with X = Cl gives a more realistic structure than with X = Cp at the present (RHF) level of calculation. In fact, Uppal et al. have proposed that ethylene inserts into the TiC bond of the intermediate, $CH_3TiCl_2^+$, based on their gas-phase experiments for the reaction of ethylene with CH_3TiCl_3.[33] Therefore, we conclude that reaction 1 with X = Cl is a good simple model for the propagation step in the homogeneous polymerization. It should be noted that the energy profile for the present model reaction is not very different from that for the reaction of ethylene with $(H_2SiCp_2)ZrCH_2^+$.[34]

II. Computational Method

We used for the geometry optimization mainly the restricted Hartree–Fock (RHF) energy gradient technique.[35] The basis functions used

(13) Cossee, P. *J. Catal.* **1964**, *3*, 80.
(14) Armstrong, D. R.; Perkins, P. G.; Stewart, J. J. P. *J. Chem. Soc., Dalton Trans.* **1972**, 1972.
(15) Novaro, O.; Chow, S.; Magnouat, P. *J. Catal.* **1976**, *42*, 131.
(16) Cassoux, P.; Crasnier, F. *J. Organomet. Chem.* **1979**, *165*, 303.
(17) McKinney, R. J. *J. Chem. Soc., Chem. Commun.* **1980**, 490.
(18) Balazs, A. C.; Johnson, K. H. *J. Chem. Phys.* **1982**, *77*, 3148.
(19) Minsker, K. S.; Zaikov, G. E. *Rev. Macromol. Chem.* **1987**, *C27*, 1.
(20) Novaro, O.; Blaisten-Barojas, E.; Clementi, E.; Giunchi, G.; Ruiz-Vizcaya, M. E. *J. Chem. Phys.* **1978**, *68*, 2337.
(21) Fujimoto, H.; Yamsaki, T.; Mizutani, H.; Koga, N. *J. Am. Chem. Soc.* **1985**, *107*, 6157.
(22) Shiga, A.; Kawamura, H.; Ebara, T.; Sasaki, T.; Kikuzono, Y. *J. Organomet. Chem.* **1989**, *366*, 95.
(23) Marynick, D. S.; Axe, F. U.; Hansen, L. M.; Jolly, C. A. *Topics in Physical Organometalic Chemistry*; Freund Publishing House, London, 1988; Vol. 3, p 37.
(24) Jolly, C. A.; Marynick, D. S. *J. Am. Chem. Soc.* **1989**, *111*, 7968.
(25) (a) Fujimoto, H.; Koga, N.; Fukui, K. *J. Am. Chem. Soc.* **1981**, *103*, 7452. (b) Fujimoto, H. *Acc. Chem. Res.* **1987**, *20*, 448.
(26) Koga, N.; Kawamura-Kuribayashi, H.; Morokuma, K. Unpublished data.
(27) Zambelli, A.; Ammendola, P.; Grassi, A.; Longo, P.; Proto, A. *Macromolecules* **1986**, *19*, 2703.
(28) Corradini, P.; Barnoe, V.; Fusco, R.; Guerra, G. *J. Catal.* **1982**, *77*, 32.
(29) Yang, X.; Stern, C. L.; Marks, T. J. *J. Am. Chem. Soc.* **1991**, *113*, 3623.
(30) Eisch, J. J.; Piotrowski, A. M.; Brownstein, S. K.; Gabe, E. J.; Lee, F. L. *J. Am. Chem. Soc.* **1985**, *107*, 7219.
(31) Upton, T. H.; Rappé, A. K. *J. Am. Chem. Soc.* **1985**, *107*, 1206.
(32) Koga, N.; Morokuma, K. *J. Am. Chem. Soc.* **1988**, *110*, 108.
(33) Uppal, J. S.; Johnson, D. E.; Staley, R. H. *J. Am. Chem. Soc.* **1981**, *103*, 508.
(34) Kawamura-Kuribayashi, H.; Koga, N.; Morokuma, K. To be submitted for publication.

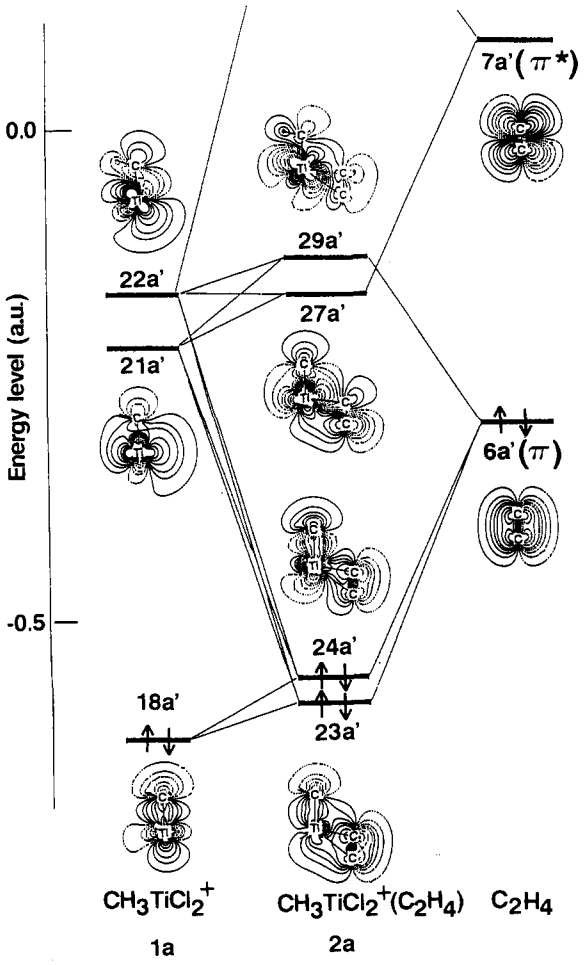

Figure 2. The orbital interaction diagram and contour maps of MOs in the C_s symmetry plane for the ethylene complex, **2a**. Only important MOs are included.

for Ti throughout the paper were MIDI4 of Huzinaga et al.[36] for the ^5F state, which were augmented by two sets of valence p functions (exponent = 0.083 and 0.028) with the overall split-valence contraction (43321/4311/31). For C, H, and Cl atoms we used the 3-21G[37,38] basis function for geometry optimization. For better energetics, we used the 6-31G basis functions,[39-41] augmented with a set of d functions (exponent = 0.8) only on the carbon atoms. The two basis sets used here are denoted I and II, respectively.

For an estimation of correlation effect and better energetics, the unrestricted second-order Møller–Plesset perturbation calculation with double spin projections (DPUMP2) was carried out and was compared with the restricted MP2 (RMP2) calculation. These MP2 calculations involve all double excitations of the valence electrons, including Ti 3s and 3p electrons.

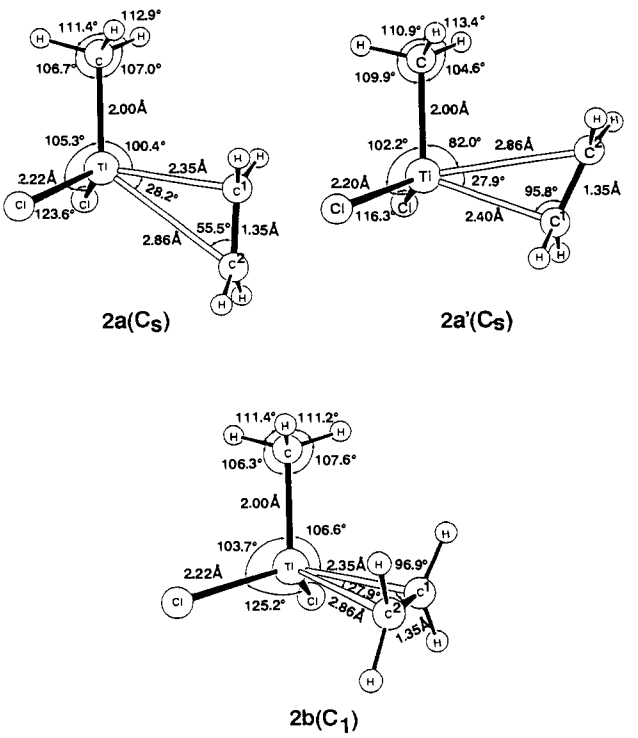

Figure 3. Optimized geometries (in Å and deg) of the ethylene complex at the RHF/I level. **2a** and **2a'** are obtained under the constraint of C_s symmetry, and **2b** without symmetry.

Table I. Olefin Binding and Relative Energies (kcal/mol) of the Ethylene Complexes $CH_3TiCl_2^+(C_2H_4)$[a]

method	2a	2a'	2b
RHF/I	−45.0 (0.0)	−43.0 (2.0)	−44.6 (0.4)
RHF/II	−41.6 (0.0)	−40.0 (1.6)	−41.2 (0.4)
UMP2/II	−45.2 (0.0)	−44.5 (0.7)	−45.2 (0.0)
DPUMP2/II	−45.3 (0.0)	−44.6 (0.7)	−45.3 (0.0)

[a] At the RHF/I optimized geometries. Energies are relative to $CH_3TiCl_2^+$ and C_2H_4. Numbers in parentheses are relative to **2a**.

III. Optimized Structures of Reactant, Intermediate, Transition State, and Product

A. Reactant: $CH_3TiCl_2^+$. The fully optimized geometries (**1a** and **1b**) of the reactant $CH_3TiCl_2^+$ under the C_s symmetry constraint are shown in Figure 1. Structure **1a** with the C–H bonds staggered to the Ti–Cl bonds is more stable by 0.9 kcal/mol (RHF/I) than **1b** with eclipsed C–H bonds. The equilibrium structure is presumed to be **1a**, whereas **1b** is a transition state for CH_3 internal rotation. One of the Ti–C–H angles in **1b** is less than 100°, a small angle similar to that in $TiCH_3(PH_3)_2Cl_3$ and an indication of the agostic interaction.[42]

Excluding high-lying but irrelevant chloride lone pair orbitals, the highest occupied molecular orbital(HOMO) is the Ti–C σ orbital, 18a', and the lowest unoccupied molecular orbitals (LUMOs) are vacant Ti d orbitals, 21a' and 22a' with a Ti–C antibonding character, as shown for **1a** in Figure 2. Both 21a' and 22a' have a large lobe at the vacant site, which can be used for easy coordination of ligands. As is often seen in coordinately unsaturated transition metal complexes, the RHF wave functions of **1a** and **1b** are found to be unstable for becoming unrestricted due to the triplet instability. An MRSDCI calculation for **1a** has confirmed that the ground state of $CH_3TiCl_2^+$ is a closed-shell singlet and that the structure **1a** is reasonable. The MRSDCI results will be published elsewhere.[26]

(35) We used the following programs and their modifications by ourselves: *GAUSSIAN82* (Binkley, J. S.; Frisch, M. J.; Defrees, D. J.; Raghavachari, K.; Whiteside, R. A.; Schlegel, H. B.; Pople, J. A. Carnegie-Mellon Chemistry Publishing Unit: Pittsburgh, PA, 1984) *GAUSSIAN86* (Frisch, M. J.; Binkley, J. S.; Schlegel, H. B.; Raghavachari, K.; Melius, C. F.; Martin, R. L.; Stewart, J. J. P.; Bobrowicz, J. W.; Rohlfing, C. M.; Kahn, L. R.; Defrees, D. J.; Seeger, R.; Whiteside, R. A.; Fox, D. J.; Fluder, E. M.; Topiol, S.; Pople, J. A. Carnegie-Mellon Chemistry Publishing Unit: Pittsburgh, PA, 1986) and *GAUSSIAN88* (Frisch, M. J.; Head-Gordon, M.; Schlegel, H. B.; Raghavachari, K.; Binkley, J. S.; Gonzalez, C.; Defrees, D. J.; Fox, D. J.; Whiteside, R. A.; Seeger, R.; Melius, C. F.; Baker, J.; Martin, R. L.; Kahn, L. R.; Stewart, J. J. P.; Fluder, E. M.; Topiol, S.; Pople, J. A. GAUSSIAN, Inc.: Pittsburgh, PA, 1988).

(36) Huzinaga, S.; Andzelm, J.; Klobukowski, M.; Radzio-Andzelm, E.; Sakai, Y.; Tatewaki, H. *Gaussian Basis Sets For Molecular Calculations*; Elsevier: Amsterdam, 1984.

(37) Binkley, J. S.; Polple, J. A.; Hehre, W. J. *J. Am. Chem. Soc.* **1980**, *102*, 939.

(38) Gordon, M. S.; Binkley, J. S.; Pople, J. A.; Pietro, W. J.; Hehre, W. J. *J. Am. Chem. Soc.* **1982**, *104*, 2797.

(39) Ditchfield, R.; Hehre, W. J.; Pople, J. A. *J. Chem. Phys.* **1971**, *54*, 724.

(40) Hehre, W. J.; Ditchfield, R.; Pople, J. A. *J. Chem. Phys.* **1972**, *56*, 2257.

(41) Hariharan, P. C.; Pople, J. A. *Mol. Phys.* **1974**, *27*, 209.

(42) Obara, S.; Koga, N.; Morokuma, K. *J. Organomet. Chem.* **1984**, *270*, C33.

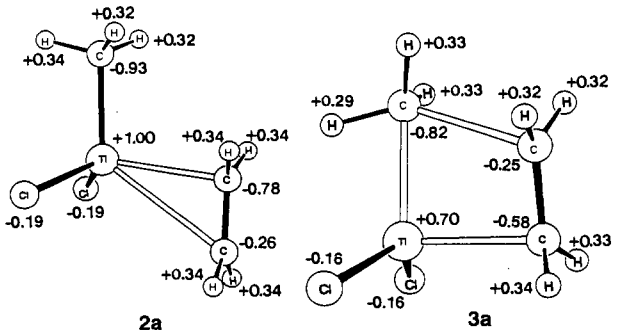

Figure 4. Atomic charge distribution of the ethylene complex, **2a**, and the transition structure, **3a**, obtained with the Mulliken population analysis at the RHF/I level.

B. Intermediate Ethylene Complex: $CH_3TiCl_2^+(C_2H_4)$. At first we optimized the geometry of $CH_3TiCl_2^+(C_2H_4)$ under the constraint of C_s symmetry, keeping Ti, three carbon atoms, and the CH_3 hydrogen atom trans to ethylene in the symmetry plane. Two optimized structures, **2a** and **2a'**, are shown at the top of Figure 3. The characters common to both are that the Ti–C bond is still 2.00 Å, unchanged from **1a**, and the length of ethylene double bond is longer only by 0.04 Å than that of the isolated molecule. The mode of ethylene coordination is different between the two; in **2a** ethylene coordinates more strongly with the carbon (C^1) closer to CH_3 with the $CTiC^1$ angle of 100°, whereas in **2a'** ethylene coordinates with the carbon (C^1) farther away from CH_3 with a $CTiC^1$ angle of 110° and ethylene as a whole is more closely situated to CH_3 than in **2a**. As shown in Table I, **2a** is more stable than **2a'** by 0.7–2.0 kcal/mol, depending on the level of calculation.

A further geometry optimization without any symmetry constraint starting slightly away from **2a** converged back to **2a**, confirming that **2a** is an equilibrium geometry. The optimization without symmetry from **2a'**, on the other hand, resulted in **2b**. Structure **2b** can be regarded as derived from **2a'** by rotating ethylene around the TiC^1 axis by the $CTiC^1C^2$ torsion angle of 100°. Structure **2a'** is the transition state of ethylene rotation between **2b** and the enantiomer of **2b** at the RHF/I level of calculation. Table I indicates, however, that the energy difference between **2b** and **2a'** is very small regardless of the level of calculation. The trans planar equilibrium structure **2a** remains more stable, only by about 1 kcal/mol, than **2a'** or **2b** at all the levels of calculation. We have to conclude that the potential surface of olefin complex is very flat with respect to ethylene rotation. If the ligands were cyclopentadienyls, structure **2b** should be very high in energy due to the steric repulsion, and **2a'** as well as **2a** would be an equilibrium structure.

There is a possibility of isomerization between **2a** and **2a'** via bond switching, i.e., tilting the C–C bond of ethylene within the C_s plane. In order to test this possibility, we optimized at the RHF/I level the structure under the constraint that the Ti–C^1 bond and Ti–C^2 bond have an equal length. The barrier for this bond switching isomerization **2a** → **2a'** thus estimated is as low as 1.4 and 1.3 kcal/mol at the RHF/II and DPUMP2/II levels, respectively.

The olefin binding energy amounts to about 40–45 kcal/mol regardless of the approximation. This large binding energy, though it must be contaminated by the basis set superposition error, can be justified by considering the coordinatively unsaturated, positively charged Ti complex interacting strongly with the electron-donating π-electron system. In solution, solvents would have been coordinating to the vacant coordination site, and thus the ethylene binding energy would be smaller. The energetics will be discussed later for the entire reaction.

The Mulliken population analysis shown in Figure 4 reveals that ethylene in the complex is substantially polarized by the positively charged Ti and at the same time that some charge transfer from ethylene to the Ti fragment has taken place.

Figure 2 shows the orbital interaction diagram for the ethylene complex **2a**, where only important orbitals and interactions are included. The occupied MO's 23a' and 24a' are in-phase and

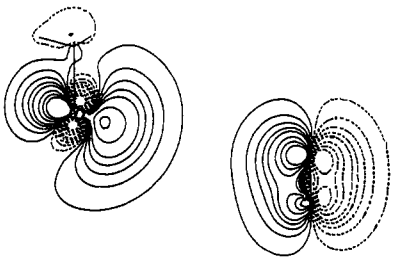

Figure 5. Contour maps of the most important paired interacting orbitals of **2a**. The contours are for ±0.01, ±0.03, ±0.05, ±0.07, ±0.09, ±0.13, and ±0.17, au, and solid and dotted lines denote positive and negative values, respectively.

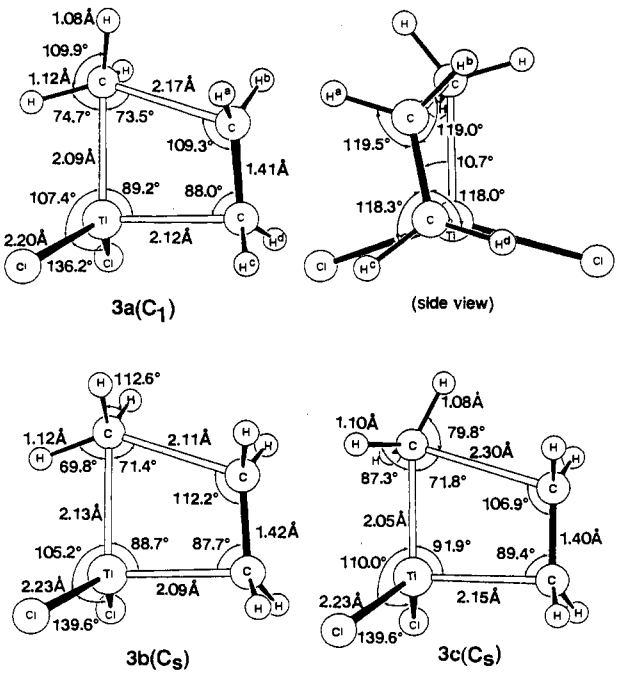

Figure 6. Optimized geometries (in Å and deg) of the "transition state" at the RHF/I level. **3b** and **3c**, determined under the C_s symmetry constraint, are not transition states. **3a** without symmetry constraint is a true transition state.

out-of-phase combinations of the ethylene π MO 6a' and the $CH_3TiCl_2^+$ occupied MO 18a', into which two vacant MO's, 21a' and 22a', of the Ti fragment mixed in due to the charge transfer interaction from ethylene to the Ti fragment. It is not very easy to see here clearly which vacant orbitals mixed with what phase. The paired interaction orbitals (PIOs), however, are the clearest way of visualizing the occupied–vacant MO interaction.[21,22] Figure 5 shows the pair of ethylene occupied and Ti fragment vacant orbital, which makes the most important contribution to the ethylene → Ti donative interaction. The ethylene PIO is the π orbital of ethylene mixed with a small fraction of the π* to be consistent with an asynchronous manner of interaction with one short Ti–C and one long Ti–C distance. The vacant PIO of the Ti fragments is essentially a nearly one-to-one mixture of 21a' and 22a', stretching as a result toward the direction of the approaching ethylene. This orbital is almost nonbonding in the Ti–CH_3 bond. This is consistent with the optimized Ti–CH_3 distance of 2.00 Å in **2a** (Figure 3) which is unchanged from that in **1a** (Figure 1).

C. Transition State: $[CH_3TiCl_2(C_2H_4)]^+$. Next we determined the transition state of this insertion reaction. At first the transition state was searched under the C_s symmetry constraint, to find two, **3b** and **3c**, shown in Figure 6. Structure **3b** with the eclipsed CH_3 is more stable by 0.44 kcal/mol at the RHF/I level than **3c**, which is very similar except for the CH_3 staggered to the ethylene CH_2. These four-centered structures are similar to those determined by Fujimoto et al.[21] and Marynick et al.[23,24] under

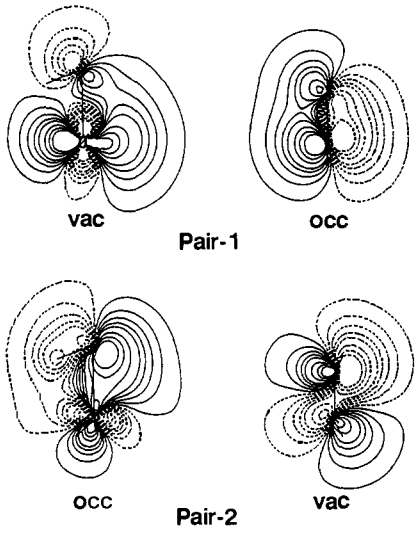

Figure 7. Contour maps of the two sets of the most important paired interacting orbitals of **3a**. See Figure 5 for contour values.

the C_s constraint. A vibrational analysis for the lower energy, eclipsed structure **3b** gives two normal modes with imaginary frequencies. One with ν = 350i cm^{-1} is a symmetric mode corresponding to the reaction coordinate for ethylene insertion into the Ti–Me bond, and the other with 157i cm^{-1} is asymmetric out-of-plane bending. Obviously neither **3b** nor **3c** is a true transition state.

A search without symmetry constraint led to the true transition state **3a**, shown in Figure 6. Structurally **3a** is similar to **3c** and in particular to **3b**. The structural features in Figure 6 indicate that **3a** is a very asynchronous transition state; the Ti–C bond, one of the two bonds being formed, is only 7% longer than in the product, whereas the CH_3–CH_2 bond, the other of the two, is still 35% longer than in the product (vide infra). The transition state is relatively early; the CH_3–Ti bond, the bond being broken, is only 4% longer than in the ethylene complex, and the CH_2–CH_2 bond distance is much closer to that in the ethylene complex than in the product. The most important difference of **3a** from the others is that the ethylene double bond is not coplanar with the Ti–CH_3 bond, with a torsional angle of 10.7°, presumably to avoid the CH_3–CH_2 eclipsing. This structure **3a** is more stable than **3b** by 0.58 kcal/mol at the RHF/I level. Although such a small energy difference may not be important in ethylene insertion, this intrinsically asymmetric transition state structure may have some importance in the stereocontrol in propylene insertion. This point will be discussed again later.

One can find a long C–H bond (1.12 Å) of the methyl group in **3a** as well as **3b**, which is an indicator of the agostic interaction. A similar long C–H bond at the transition state has also been found by Fujimoto et al.[21] The fact that **3b** with the eclipsed CH_3 is more stable than **3c** with the staggered CH_3 is ascribable to this agostic interaction. The α C–H agostic interaction during the chain propagation step has been proposed to assist olefin insertion.[43] In the recent experiments by Piers and Bercaw, the α C–H agostic interaction has been shown to assist the C–C bond formation in hydrocyclization of hexadiene.[44] Marynick et al. have also found that the eclipsed transition state is more stable than the staggered one in the reaction of X = Cp.[24] However, they have ascribed this to the nonbonded interaction between Ti and CH_3.

In order to illustrate important orbital interactions at the transition state, we have carried out the PIO analysis at the coplanar "transition state" **3b**, whose electronic structure is similar to that of **3a** and can be analyzed more easily than **3a** owing to its C_s symmetry. As shown in Figure 7, the most important PIO pair-1 consists of the polarized π orbital of C_2H_4, and the vacant d_{z^2}-like orbital of $CH_3TiCl_2^+$. This pair is similar to the PIO pair for the ethylene complex (Figure 5), but the polarization and reorganization have taken place more strongly here than in Figure 5. For instance, the $CH_3TiCl_2^+$ fragment orbital is more strongly Ti–CH_3 antibonding and the ethylene π orbital is much less C–C bonding. As a result, this ethylene → Ti donative interaction represents the cleavage of the Ti–CH_3 and the C–C π bond, as well as the Ti–C^α bond formation. The pair-2 represents back-donation from the Ti–CH_3 σ orbital to the ethylene π^* orbital to promote the CH_3–C^β bond formation and the Ti–CH_3 and ethylene π bond cleavage. These two pairs thus give an orbital justification for smooth bond switching in the insertion reaction.

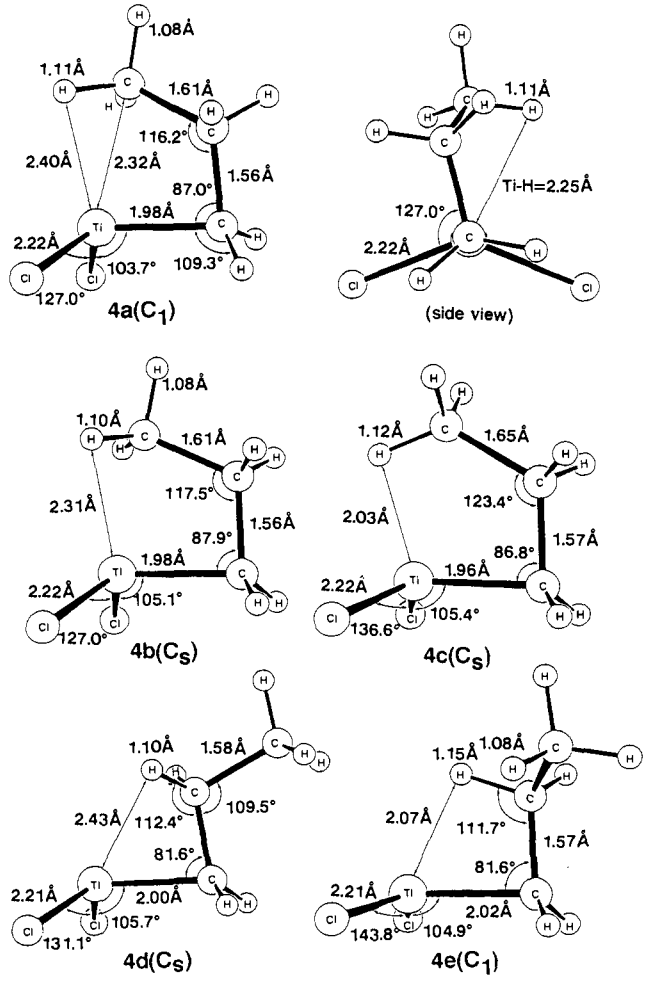

Figure 8. Optimized geometries (in Å and deg) of the propyl complex at the RHF/level. **4b**, **4c**, and **4d** are obtained under the C_s symmetry constraint, and **4a** and **4e** without constraint.

The atomic charges of **3a**, shown in Figure 4, indicate that C^β is more cationic by 0.3 e than C^α. This suggests that the replacement of one hydrogen on C^β by an inductively electron donating methyl group will give a more stable transition state of olefin insertion than the replacement on C^α, in accordance with the Markovnikov rule. This point will be discussed again later.

D. Product: $C_3H_7TiCl_2^+$. In this section, we discuss the optimized geometries of the product propyl complex. From the results of the reactant methyl complex, one expects that structures with agostic interactions are the most stable. As shown in Figure 8, structural optimization with C_s symmetry constraint yielded three optimized structures: **4b** and **4c** with γ C–H agostic interaction and **4d** with β C–H agostic interaction. **4c** has both $C^\alpha H_2$–$C^\beta H_2$ and $C^\beta H_2$–$C^\gamma H_3$ eclipsed, and is, as shown in Table II, less stable than **4b** which has $C^\alpha H_2$–$C^\beta H_2$ eclipsed but $C^\beta H_2$–$C^\gamma H_3$ staggered. To avoid the eclipsed $C^\alpha H_2$–$C^\beta H_2$ maintaining the $C^\gamma H_3$ agostic interaction, one has to break the

(43) (a) Brookhart, M.; Green, M. L. H. *J. Organomet. Chem.* **1983**, *250*, 395. (b) Brookhart, M.; Green, M. L. H.; Wong, L. *Prog. Inorg. Chem.* **1988**, *36*, 1.

(44) Piers, W. E.; Bercaw, J. E. *J. Am. Chem. Soc.* **1990**, *112*, 9406.

Table II. Energies (kcal/mol) of Propyl Complexes Relative to the Ethylene Complex **2a**[a]

with C^{γ}–H and C^{β}–C^{α} agostic interaction		with C^{β}–H agostic interaction	
4a	−45.0 (0.0)	**4d**	−40.6 (4.4)
4b	−44.9 (0.1)	**4e**	−40.3 (4.7)
4c	−38.0 (7.0)		

[a] Energy at the RHF/I level at the RHF/I optimized geometries. Numbers in parentheses are relative to **4a**.

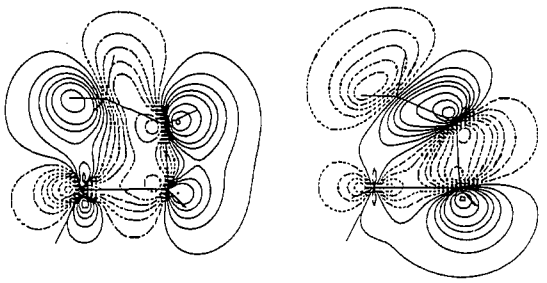

31 32

Figure 9. Contour maps of occupied canonical MOs 31 and 32 of **4a**. See Figure 5 for contour values.

C_s symmetry. In fact, geometry optimization without symmetry constraint gave a single optimized structure **4a**, which is believed to be the most stable geometry of the product (Table II). One can see in Figure 8 that all the single bonds in **4a** are more or less staggered, presumably the origin of the stability. The structural features of **4a**, as well as **4b** and **4c**, are interesting. The Ti–C^{α}–C^{β} angles are smaller than 90.0°, the C–H bonds involved in the agostic interaction are longer than the normal C–H bond, and, in addition, the C^{β}–C^{γ} bond is stretched more, by about 3%, than the normal C–C bond. These features indicate that the C^{β}–C^{γ} as well as the C^{γ}–H agostic interaction is taking place. We show contour maps of two molecular orbitals, 31 and 32, of **4a** in Figure 9, which demonstrate the existence of such interaction. MO 32 indicates the donative interaction from both C^{α}–C^{β} and C^{β}–C^{γ} bonds to a Ti d orbital, and MO 31 represents the donation from the C^{β}–C^{γ} bond and the C^{γ}–H bond to a Ti d orbital. These features are very similar to and agree with our previous report on $Ti(C(SiH_2CH_3)=CH_2)X_2^+$.[42]

In addition to **4d**, we obtained a nonsymmetric optimized structure **4e** which has a C^{β}–H agostic interaction and the eclipsed C^{α}–C^{β} conformation. The two structures are similar in energy, presumably due to the cancellation of stronger C^{β}–H agostic interaction of **4e** and more favorable staggered conformation of **4d**. However, both are less stable by 4.4–4.7 kcal/mol than **4a** at the RHF/I level. Though we have not studied the origin of this energy difference in detail, presumably the cationic, coordinatively unsaturated Ti would prefer to interact with two donors, the C^{β}–C^{γ} and C^{γ}–H bond, rather than one donor, C^{β}–H bond. We would also like to mention that geometry optimization starting with the C^{α}–C^{β} bond away from the Ti vacant site, i.e., with $TiCl_2$ and C^{α}–H_2 staggered, caused the $TiCl_2$ moiety to invert, to result in one of the above optimized structures.

IV. Energetics of Ethylene Insertion

In this section we discuss the energetics of ethylene insertion reaction, eq 1, in detail. Energies of the most stable structures of the reactant complex, **2a**, the transition state **3a** and the product **4a**, relative to the reactants, at various levels of calculation are shown in Table III. Potential energy profiles at a few levels are also illustrated in Figure 10. Here DPUHF and DPUMP2 refer to the UHF and the UMP2 wave functions, respectively, in which both the triplet and the quintet components are projected out.[45]

(45) The values used in Tables III and IV came from the single annihilation.[46] Though the single annihilation can cause an error with the projection of only the $S + 1$ state,[47] it gives a correct estimate when two spin states, $S + 1$ and $S + 2$, are projected out (Koga, N.; Yamashita, K.; Morokuma, K. *Chem. Phys. Lett.* **1991**, *184*, 359).

Table III. Relative Energies, Activation Energies and Energy of Reaction (kcal/mol) for Ethylene Insertion into $CH_3TiCl_2^+$ at Various Levels[a]

method	ethylene complex **2a**	transition state **3a**	activation energy **3a**–**2a**	product **4a**	energy of reaction **4a**–**2a**
RHF/I	−45.0	−33.7	11.3	−47.4	−2.4
UHF/I	−43.0	−31.7	11.3	−46.8	−3.8
UMP2/I	−44.0	−34.9	9.1	−49.3	−5.3
RHF/II	−41.5	−27.7	13.8	−45.0	−3.5
UHF/II	−39.0	−25.1	13.9	−43.7	−4.7
DPUHF/II	−39.3	−31.2	8.1	−44.3	−5.0
RMP2/II	−45.5	−39.9	5.6	*b*	
UMP2/II	−45.2	−35.8	9.4	−50.5	−5.3
DPUMP2/II	−45.3	−41.0	4.3	−56.4	−11.1

[a] At the RHF/I optimized geometries. Energies are relative to $CH_3TiCl_2^+$ and C_2H_4. [b] The relative energy of **4a** is less than −400 kcal/mol, apparently diverging due to the improper RHF wave function.

Table IV. Expectation Values $\langle S^2 \rangle$ of Unrestricted Wave Functions for Ethylene Insertion into $CH_3TiCl_2^+$ at Various Levels[a]

method	reactant **1a**	ethylene complex **2a**	transition state **3a**	product **4a**
UHF/II	0.639	0.561	0.654	0.595
DPUHF/II	0.000	0.000	0.003	0.000
UMP2/II	0.583	0.501	0.555	0.532
DPUMP2/II	0.000	0.000	0.000	0.000

[a] At the RHF/I optimized geometries.

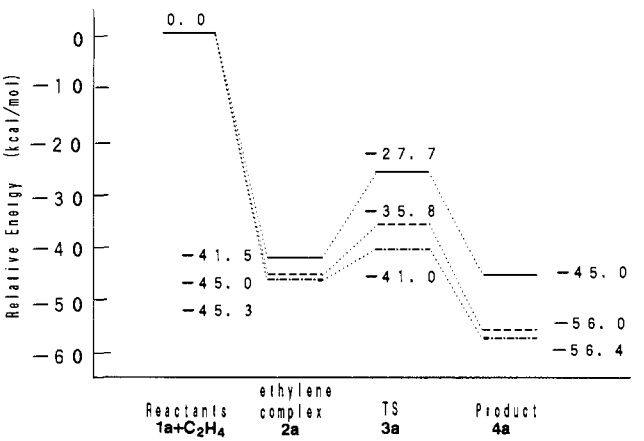

Figure 10. Potential energy profiles of ethylene insertion process at various levels: (—) RHF/II, (--) UMP2/II, and (-·-) DPUMP2/II.

As shown in Table IV, UHF and UMP2 wave functions have large S^2 expectation values, up to 0.65, a clear sign of large higher-spin contamination. After the double projection, S^2 expectation values almost converge to zero. Therefore, the DPUMP2 method is considered to be good semiquantitative energetics.

The relative energy of **2a**, the negative of ethylene coordination energy, is not very sensitive to the basis set, the correlation, or the spin restriction (restricted or unrestricted) and projection. The better basis set decreases and the correlation increases the binding energy by a few kcal/mol. The spin projection has little effect.

The energy of reaction, **4a** or **4a**–**2a**, depending on what is taken as the "reactant", is not sensitive to the basis set or the spin projection. However, the electron correlation makes the reaction more exothermic. An RMP2 calculation for **4a** gave an unrealistic energy, presumably due to the small HOMO–LUMO gap, a case where the RHF wave function may not be appropriate.

(46) Schlegel, B. H. *J. Chem. Phys.* **1986**, *84*, 4530; *J. Phys. Chem.* **1988**, *92*, 3075.

(47) Knowles, P. J.; Handy, N. C. *J. Chem. Phys.* **1988**, *88*, 6991; *J. Phys. Chem.* **1988**, *92*, 3097.

Scheme II

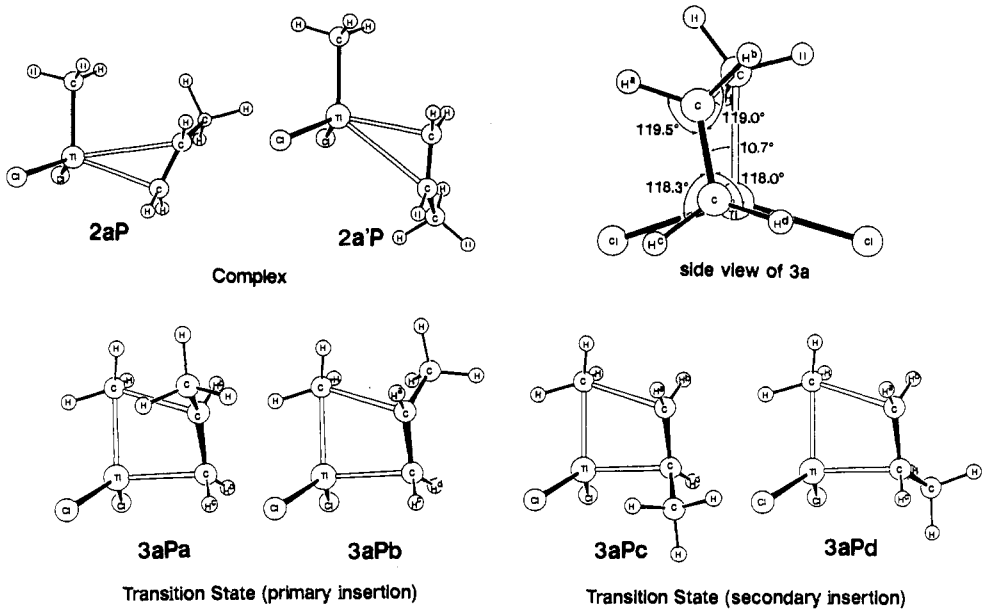

Table V. Relative Energies (kcal/mol) for Ethylene (R = H) and Propylene (R = CH_3) Insertion Reactions, Eq 1[a]

	olefin complexes		transition states	
ethylene	**2a**	−45.0	**3a**	−33.7 (11.3)
	2a'	−43.0		
propylene	**2aP**	−52.6	**3aPa**	−35.8 (17.8)
	2a'P	−50.0	**3aPb**	−33.6 (19.0)
			3aPc	−27.1 (25.5)
			3aPd	−31.2 (21.4)

[a] Energies in kcal/mol at the RHF/I level, at the RHF/I optimized geometries for ethylene reaction, combined with the standard geometry of CH_3. Energies are relative to $CH_3TiCl_2^+$ and ethylene or propylene. Numbers in parentheses are activation energies from the most stable olefin complexes.

The energy of the transition state, on the other hand, is sensitive to the correlation as well as to the spin unrestriction and projection. The correlation lowers the barrier height by 4–8 kcal/mol, and the spin projection by about 5 kcal/mol. The best estimation of the barrier from the most stable ethylene complex is 4.3 kcal/mol. This result is in good agreement with the experimental estimate of activation energy of 6–12 kcal/mol for similar systems.[48-50] The insertion reaction is indeed a very easy process.

V. An Application to Propylene Insertion

As a first step of studying the insertion of propylene to $CH_3TiCl_2^+$, we replaced, without further geometry optimization, one of the C_2H_4 hydrogen atoms in the reactant complexes **2a** and **2a'** and in the transition state **3a** by a methyl group having a standard geometry taken from the optimized structure of propylene and having a conformation eclipsed (in **2a** and **2a'**) or staggered (in **3aP**'s) with the C=C bond. We illustrate in Scheme II the propylene complexes, **2aP** and **2a'P**, and the transition state for primary insertion, **3aPa** and **3aPb**, and those for secondary insertion, **3aPc** and **3aPd**, as well as the side view of **3a** indicating the direction of the hydrogen atoms to be replaced.

Propylene complexes, **2aP** and **2a'P**, are two of the most stable of the possible model complexes. Actually we have confirmed that the other models, in which the methyl group is attached to C^1 in **2a** or **2a'**, are less stable by more than 5 kcal/mol than **2a'P**, presumably due to steric repulsion. In addition, C^2 is more cationic than C^1, as shown in Figure 4, and thus methyl substitution on C^2 is more favorable. Table V shows that the binding energies of formation of the propylene complexes, **2aP** and **2a'P**, are larger by 7–8 kcal/mol than those of the corresponding ethylene complexes. The energy decomposition analysis (EDA) shown in Table VI indicates that this increment is mainly due to the increase in the electrostatic attraction between the Ti fragment and olefin. The electron-donative CH_3 group makes the propylene carbons more negatively charged. This attraction is supplemented further by enhanced donative and back-donative attractive interactions. Between the two propylene complexes, **2aP** is more stable than **2a'P** by 2.6 kcal/mol. This energy difference is essentially the same as that between **2a** and **2a'**, and the EDA results in Table VI, confirm that the **2a**–**2a'** difference is indeed the origin of the **2aP**–**2a'P** difference.

Table VI. Energy Decomposition Analysis of the Interaction between $CH_3TiCl_2^+$ and C_2H_4 or C_3H_6 in Olefin Complexes[a]

	C_2H_4		C_3H_6	
	2a	**2a'**	**2aP**	**2a'P**
CTPLX (Ti → L)[b]	−20.3	−16.8	−22.9	−19.3
CTPLX (L → Ti)[c]	−25.6	−24.4	−27.0	−25.9
ES	−30.1	−28.9	−34.4	−32.6
EX	26.8	24.1	28.5	25.8
res	−0.1	−0.6	−0.8	−1.6
total interaction	−49.3	−46.6	−56.6	−53.6
deform. energy[d]	4.3	3.6	4.0	3.6
total	−45.0	−43.0	−52.6	−50.0

[a] Energies in kcal/mol at the RHF/I level. [b] This energy term represents the back-donative interaction, which includes the charge transfer (CT) from the occupied orbitals of $CH_3TiCl_2^+$ to the vacant orbitals of olefin, and the polarization (PL) in the latter. [c] This term represents the donative interaction, which includes CT from occupied orbitals of olefin to the vacant orbitals of $CH_3TiCl_2^+$ and PL in the latter. [d] The deformation energy of $CH_3TiCl_2^+$ and olefin.

The calculated energetics in Table V indicates that the insertion of propylene starting from the complex requires a larger activation energy than that of ethylene. Table V also shows that the two transition states **3aPa** and **3aPb**, giving the primary insertion (head-to-tail) products, are lower in energy than **3aPc** and **3aPd**, leading to the secondary insertion (tail-to-head) products. These theoretical results of chemo- and regioselectivity are in good qualitative agreement with experimental observations.[1-4] Table V indicates that the higher barrier for propylene insertion is due to the fact that propylene complexes, **2aP** and **2a'P**, have larger stabilization energies than ethylene complexes, **2a** and **2a'**, while the transition states, **3aPa** and **3aPb**, have a stabilization energy

(48) Natta, G.; Pasquon, I. *Adv. Catal.* **1959**, *11*, 1.
(49) Machon, J.; Hermant, R.; Houteaux, J. P. *J. Polym. Sci. Symp.* **1975**, *52*, 107.
(50) Chien, J. C. W. *J. Am. Chem. Soc.* **1959**, *81*, 86.

Table VII. Energy Decomposition Analysis of the Interaction between $CH_3TiCl_2^+$ and Olefin at the Assumed Transition States[a]

	ethylene	propylene			
		primary		secondary	
	3a	**3aPa**	**3aPb**	**3aPc**	**3aPd**
CTPLX (Ti → L)	−41.8	−44.5	−44.5	−47.1	−46.2
CTPLX (L → Ti)	−62.8	−63.5	−63.4	−66.0	−65.5
ES	−91.0	−99.5	−100.2	−96.7	−94.7
EX	132.8	144.9	148.0	155.3	148.0
res	−4.6	−8.7	−8.8	−8.5	−8.5
total interaction	−67.2	−71.3	−69.1	−63.0	−67.0
deform. energy	33.5	35.5	35.5	35.9	35.8
total	−33.7	−35.8	−33.6	−27.1	−31.2

[a] Energies in kcal/mol at the RHF/I level. For the definition of energy terms, see Table VI.

similar to that of **3a**. The EDA analysis in Table VII suggests that the similar stabilization energy for **3aPa** or **3aPb** relative to **3a** is due to cancellation of the increased exchange repulsion and the increased electrostatic attraction.

The EDA analysis in Table VII also provides a clue to the origin of regioselectivity. The transition states for primary insertion, **3aPa** and **3aPb**, are energetically more favored than those for secondary insertion, **3aPc** and **3aPd**, mainly again due to the more favorable electrostatic attraction and less serious exchange repulsion. The Mulliken population analysis suggests that propylene at the transition state develops about 0.2 e more negative charge on the carbon away from CH_3 and 0.2 e less on the carbon next to CH_3 in comparison with ethylene. This gives a more favorable electrostatic interaction for primary insertion than for secondary insertion. In the transition states for secondary insertion, the methyl group of propylene is more closely located to the bulky Cl ligands than for primary insertion, causing a larger exchange repulsion.

Now we can discuss the stereoselectivity of propylene insertion. Of the two transition states for primary insertion, **3aPa** is lower in energy than **3aPb** by about 2.2 kcal/mol at the RHF/I level as shown in Table V. A 4-kcal/mol difference is found between two transition states for secondary insertion. These significant differences in activation energy favoring one stereospecificity to the other are caused entirely by the slight nonplanarity of the present four-centered transition state. Of course, this stereoselectivity has no practical meaning for this model insertion reaction, since the sense of nonplanarity starting from totally nonchiral reactants is random. However, the tendency of the four-centered transition state to be nonplanar by itself may have a substantial significance in the stereospecificity of olefin polymerization in which the reactant, the growing end of a polymer chain, can already by chiral.[27] As shown in Table VII, the exchange repulsion energy is the origin of these energy differences. As one can clearly see in the side view in Scheme II, the methyl group of propylene in **3aPa** is in a much less crowded region than in **3aPb**. For secondary insertion, in the less stable **3aPc** the methyl group of propylene is more closely located to the bulky chlorine and therefore sterically more hindered than in the more stable **3aPd**.

VI. Conclusions

We have studied the reaction mechanism of ethylene insertion into the titanium carbon bond of $CH_3TiCl_2^+$ with the ab initio molecular orbital method. We have found two forms of ethylene complex, one with the ethylene C–C bond coplanar and another perpendicular to the Ti–CH_3 bond. They have nearly equal energy at the best DPUMP2/II//RHF/I level. The potential surface is very flat for changes in coordination direction in the ethylene complex. The transition state is four-centered and nonplanar, with a CTiCC dihedral angle of 10.7°. The activation energy from the ethylene complex is very sensitive to the method of calculation, i.e., the correlation as well as the spin unrestriction and projection, and is about 4 kcal/mol at the best level. This model insertion should take place easily, as is suggested experimentally. In the product, there is a strong C^{β}–C^{γ} and C^{γ}–H agostic interaction with Ti vacant orbitals. We have also found that the insertion of propylene is more difficult than that of ethylene, and the primary insertion takes place more easily than the secondary insertion. Both of these chemo- and regioselectivities have been found by an energy decomposition analysis to be controlled by changes in steric repulsion and electrostatic attraction. Because of the nonplanarity of the transition state for ethylene insertion, one transition state for primary insertion of propylene giving one stereospecificity has a lower activation energy by 2 kcal/mol than the other, giving the opposite stereospecificity. This intrinsic nonplanarity of transition state has no practical influence in the insertion to nonchiral $CH_3TiCl_2^+$, since the sense of nonplanarity induced in this model system is random. However, this would play a very important role in the chain growth step of polymerization where the conformation of R in $RTiCl_2^+$ would dictate the sense of nonplanarity at the transition state. This aspect of stereocontrol in propylene polymerization is presently under investigation.

Acknowledgment. All numerical calculations were carried out at the Computer Center of IMS. The authors thank Dr. K. Yamashita for helpful discussions. H. Kawamura-Kuribayashi was a visiting scientist trainee at IMS when this work was carried out. Acknowledgment is also made to the Ministry of Education, Science and Culture for grant-in-aid.